EFFECT OF FINISH ROLLING AND QUENCH STOP TEMPERATURES ON IMPACT-ABRASIVE WEAR RESISTANCE OF 0.35 % CARBON DIRECT-QUENCHED STEEL

O. Haiko[1*], I. Miettunen[1], D. Porter[1], N. Ojala[2], V. Ratia[2], V. Heino[2], A. Kemppainen[3]

[1]University of Oulu, Faculty of Technology, Materials Engineering and Production Technology, P.O.Box 4200, 90014 Oulu, Finland.

[2]Tampere University of Technology, Department of Materials Science, Tampere Wear Center, P.O.Box 589, 33101 Tampere, Finland.

[3]SSAB Europe, P.O.Box 93, 92101 Raahe, Finland

ABSTRACT

Novel high-hardness medium-carbon martensitic laboratory steel has been produced and tested for abrasive wear resistance. Different finish rolling temperatures (FRT) combined with either direct quenching (DQ) or interrupted quenching to 250 °C was applied to vary the content of retained austenite and hardness. The steel carbon content was set to 0.35 % to obtain a surface hardness of approximately 600 HB. Lowering the finish rolling temperature in the range 920–780 °C, i.e. into the non-recrystallization regime resulted in a more elongated prior austenite grain structure, which increased the hardness of the DQ variants without any significant loss of Charpy-V impact toughness. Although increasing the degree of autotempering by raising the quench stop temperature reduces the hardness of the martensitic microstructure, it was found that proper quenching stop temperature could be utilized to achieve balanced toughness and hardness properties. Impact-abrasive wear resistance as measured in impeller-tumbler tests with natural granite as the abrasive demonstrated that wear resistance increased with increasing surface hardness.

Keywords: wear, steel, impact abrasion, hardness

*Corresponding author: Oskari Haiko (oskari.haiko@oulu.fi)

INTRODUCTION

Abrasive and impact wear are often present in the severe conditions of mining, mineral processing, earth-moving and agricultural industries. Rocks, sand and gravel cause heavy wear by sliding, impacting or grooving on the surface subjected to wear. High-hardness steels are commonly used as wear-resistant materials in many applications. The wear resistance is often considered to be related to the surface hardness of the steel. Commercial wear-resistant steels are available in different hardness grades ranging from 400 up to 600 HB. The higher hardness is usually obtained by increasing the carbon content of the steel. However, the higher carbon content normally leads to limited usability. Toughness, bendability and weldability properties are deteriorated. Hence, other methods are also implemented to increase the hardness of steel without drastic loss of other important properties.

Direct quenching (DQ) has been utilized for producing similar steels with leaner alloying.

Thermomechanically controlled processing (TMCP) has been introduced for refining the grain size. Both of the processing methods are nowadays used for production of ultra-high strength steels [1–3]. Finer grain size is obtained by controlled rolling in the non-recrystallization regime (NRX). Strain is applied to the austenite, which leads to increased dislocation density and an elongated grain structure. Finish rolling temperature (FRT) should be low enough for reduction to take place in the NRX regime. Direct quenching is then applied after the finishing pass. This approach gives increased strength and toughness without a major loss of ductility [2].

The balance between impact toughness and hardness is often a trade-off in high-hardness steels. Super high-hardness steels may exhibit very low impact toughness values below room temperature. Adopting TMCP and DQ improves the impact toughness, but transition temperatures might still remain relatively high. In earlier research, an attempt to solve this problem was made by introducing small amounts of ferrite into the martensitic matrix [4]. However, it was difficult to control the amount of ferrite and this approach was dismissed. Hence, a new cooling method was applied to improve the impact toughness properties. Water quenching was interrupted at 250 °C after which the rolled plates were cooled in still air. Quenching finish temperature (QFT) was set between the martensite start (M_s) and finish (M_f) temperatures. The aim was to induce autotempering effects and possibly increase the retention of some austenite to improve the impact toughness [5–7].

As regards the selection of an abrasive wear test to simulate the conditions experienced in excavation and rock moving applications, the impeller-tumbler wear testing is appropriate [8]. This apparatus is an impact-abrasion wear tester that allows the use of natural granite as the abrasive. Materials are subjected to heavy surface deformation during testing. Mass loss of the specimens is measured during and after the wear testing.

MATERIALS AND METHODS

Materials and laboratory rolling experiments

The purpose of the work was to investigate the effect of different rolling and quenching parameters on wear resistance. The chemical composition of the laboratory steel is presented in Table 1. The carbon content of 0.35 % was estimated to be sufficient to produce martensite with a hardness of 600 HB after hot rolling and direct quenching [9]. The composition was designed to have a good balance of strength, hardness and impact toughness as well as wear resistance together with good usability and ease of production.

The slab annealing temperature was 1200 °C for 2 hours to produce a uniform grain size. The slab size was 140 × 80 × 60 mm. Slabs were rolled from 60 mm to final thickness of 9 mm with total reduction of 85 %. The hot rolling schedule included three different finish rolling temperatures (FRT) 920, 850 and 780 °C to vary the degree of rolling below the non-recrystallization temperature (T_{nr}), which was estimated to be around 950 °C on the basis of the equation given by Barbosa et al. [10]. The temperature during hot rolling and cooling was monitored with an ANSI type K thermocouple. A hole was drilled in the middle of the slabs to be fitted with the thermocouple prior to rolling.

Table 1. Chemical composition of the laboratory steel (wt.%, balance Fe).

C	Si	Mn	Al	V	Ti	Cr	Ni	Mo
0.349	0.250	0.510	0.033	0.0014	0.0028	0.770	2.000	0.150

The rolled plates were direct quenched immediately after the final rolling pass. The calculated M_s temperature of the steel was 325–330 °C [9]. Quenching was either continued to room temperature or interrupted at 250 °C with the aim of producing different fractions of retained austenite. The steel plates were submerged into a water tank equipped with water circulation to maximize the cooling rate. Therefore, the severity of quench was high. Once the required quenching finish temperature (QFT) was reached, the water quenching was halted by removing the plates from the tank after which they were cooled in still air. The realized quenching finish temperatures were then inspected from the thermocouple data.

Microstructural characterization and mechanical testing

Optical and electron microscopes were utilized for microstructural characterization. A Keyence VK-X200 microscope was used for study of the prior austenite grain size, microstructure and wear surfaces. More detailed microstructural inspection was carried out with a Zeiss Sigma field emission scanning electron microscope (FESEM). The samples were polished and etched with picric acid, for studying prior austenite grain size, or 4 % Nital for studying the martensitic microstructure. The prior austenite grain size was measured using the linear intercept method from planar sections [11].

X-ray diffraction (XRD) analysis is typically used in determining the amount of retained austenite in carbon steels. The present measurements were done by a Rigaku SmartLab X-ray diffractometer with a rotating Co anode X-ray tube as a radiation source. The equipment was operated at 135 mA and 40 kV setting. In order to eliminate the effect of texture and collect the correct intensities of the phases, a so-called detexturation measurement was performed. In this procedure, a specimen was tilted by steps of 5° up to angle of 70° (i.e. the χ axis varied from 0° to 70°) and simultaneously rotated 360° around the φ axis. Each scanning was carried out with a 0.1° stepping over a 2θ range from 45° to 130°. The total scanning time was 100 minutes. The volume fractions of retained austenite were calculated from the X-ray data by Rietveld's whole powder profile fitting method using commercially available PDXL2 software and R_{wp} values were less than 10.

Mechanical testing included only hardness and impact toughness measurements due to the small amount of material produced. Surface hardness was measured with a Struers Duramin A-300 hardness tester. The load was 10 kg and Vickers HV hardness scale was used. The hardness of 600 Brinell corresponds to 630–640 in Vickers HV10 scale. Surface hardness was measured from the prepared wear test samples prior to wear testing. Two millimetres were machined off from the surface and five indentations per sample were measured across the surface. Material bulk hardness profiles were measured through the thickness of the rolled plates with HV10 and 0.5 mm steps between indentations. Charpy-V testing in the temperature range of -80 to 120 °C was conducted for measuring the impact toughness and determining the transition temperature. Two 10 × 7.5 × 55 mm samples oriented parallel to the rolling direction were tested for each temperature and steel variant. Impact testing was not continued to lower temperatures if the impact energy did not reach 20 joules.

Wear testing

Wear testing was conducted using the facilities at Tampere Wear Center (TWC) in Tampere University of Technology, Finland. The steels were tested with an impeller-tumbler that simulates heavy impact-abrasive wear [8]. The apparatus includes the impeller part with sample holder and a 350 mm diameter tumbler, in which gravel is placed. Both parts rotate in the same direction. Samples are attached to the impeller sample holder that can hold three samples at a time. One of the samples is a reference sample. The impeller rotates inside the tumbler and samples hit the abrasives with a high velocity. The tumbler keeps the gravel moving and impacting the samples. Here, the impeller rotation speed was set to 700 rpm and the tumbler 30 rpm, respectively.

Samples were oriented at an angle of 60° to the sample holder perimeter. Since the abrasives are loose inside the tumbler the abrasives do not necessarily impact the sample at the sample angle. Natural granite in the size range of 10–12.5 mm was used as the abrasive material. Each batch of abrasives had a mass of 900 g. Gravel was renewed and the mass loss of the samples was measured at 15 min intervals during the total test time of 60 min. Before the actual test, the testing procedure included a 15 min running-in phase to reach steady-state wear. Of the three sample slots, the two actual test material samples were rotated between slots 1 and 2 at every 15 minutes, but the reference material was kept in slot 3 throughout the test for comparability. The sample size was 71 × 24 × 7.8 mm and two samples were tested per variant. An illustration of the device is presented in Figure 1.

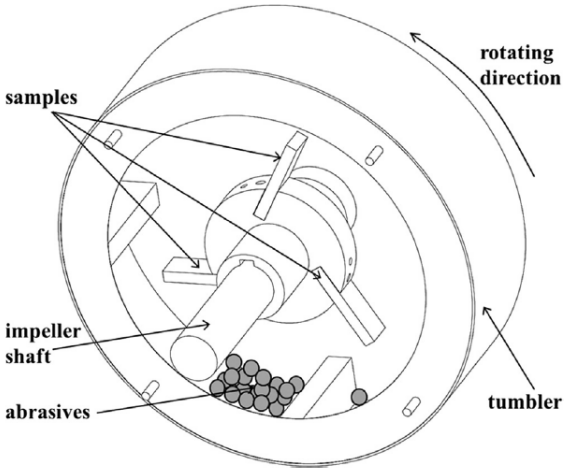

Figure 1. Impeller-tumbler wear testing device illustrated [8].

RESULTS

Microstructures

The prior austenite grain size and structure is clearly different between the tested steels. Figure 2 shows the effect of decreasing finish rolling temperature. The direct quenched plates are referred as DQ variants and the plates with interrupted quenching are referred as QFT variants or identified with the code "250", i.e. the aim QFT. Grain structure is more pancaked in the lower FRT samples. Controlled rolling in the non-recrystallization regime has produced a more distorted grain structure: the austenite grains are flattened and elongated. The prior austenite grain size was determined using the linear intercept method described by Higginson et al. [11], i.e. in the plate normal and rolling directions, see Table 2. The aspect ratio of the grains increases drastically with decreasing finish rolling temperature, while the overall mean grain size stays nearly the same for 780 and 920 FRT variants. Thus, the grain structure might be very distorted or nearly equiaxed with the same overall mean linear intercept. Nevertheless, the more distorted and elongated grain structure may exhibit higher grain boundary area per unit volume (S_v) and increased dislocation density.

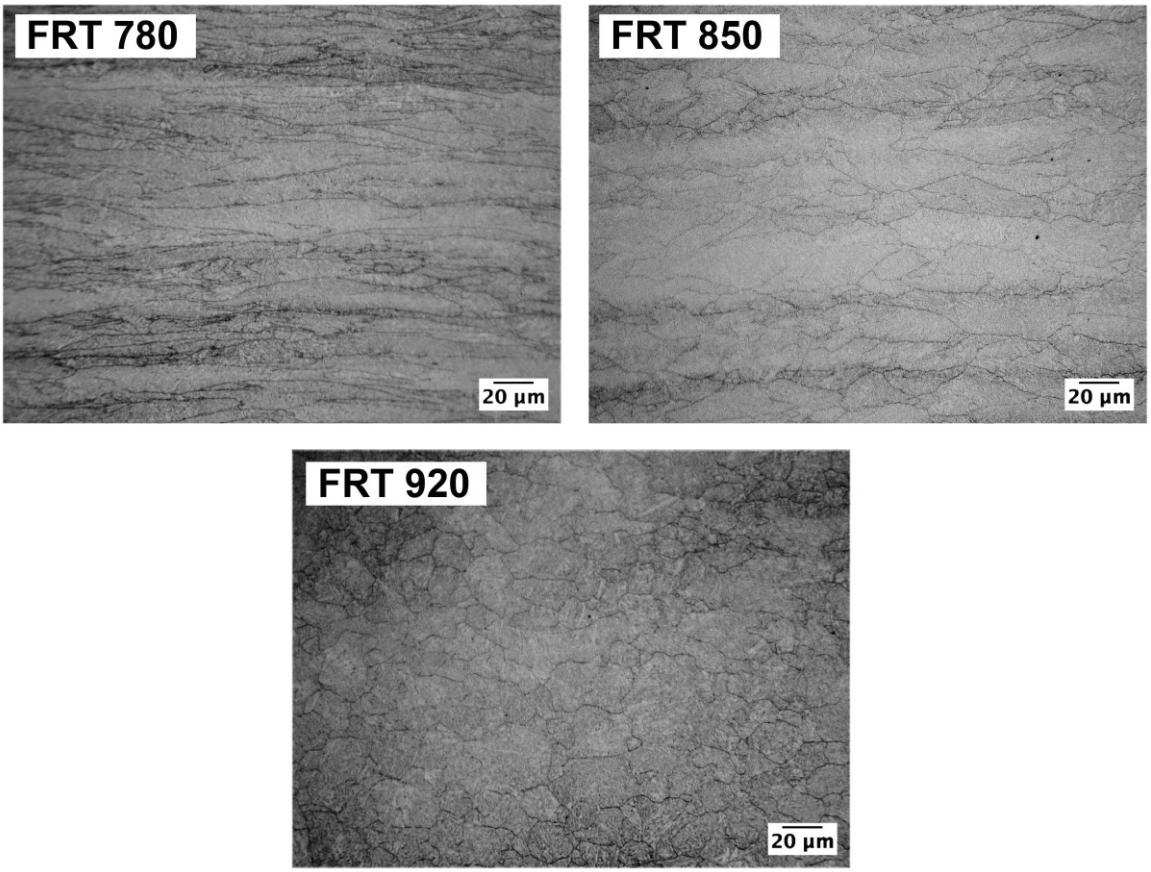

Figure 2. Optical microscope images of the samples etched to reveal prior austenite grain size with different finish rolling temperatures (FRT).

Table 2. Mean prior austenite grain size. ND is normal and RD rolling direction, AR stands for aspect ratio and L is the mean linear intercept value. ± values are 95 % confidence intervals for the mean.

FRT	L_{ND} (µm)	L_{RD} (µm)	AR	L (µm)
780	7.83±0.65	32.65±2.96	4.17	15.99±3.08
850	12.63±1.04	29.28±2.68	2.32	19.23±2.86
920	13.09±1.13	18.43±1.59	1.41	15.53±1.70

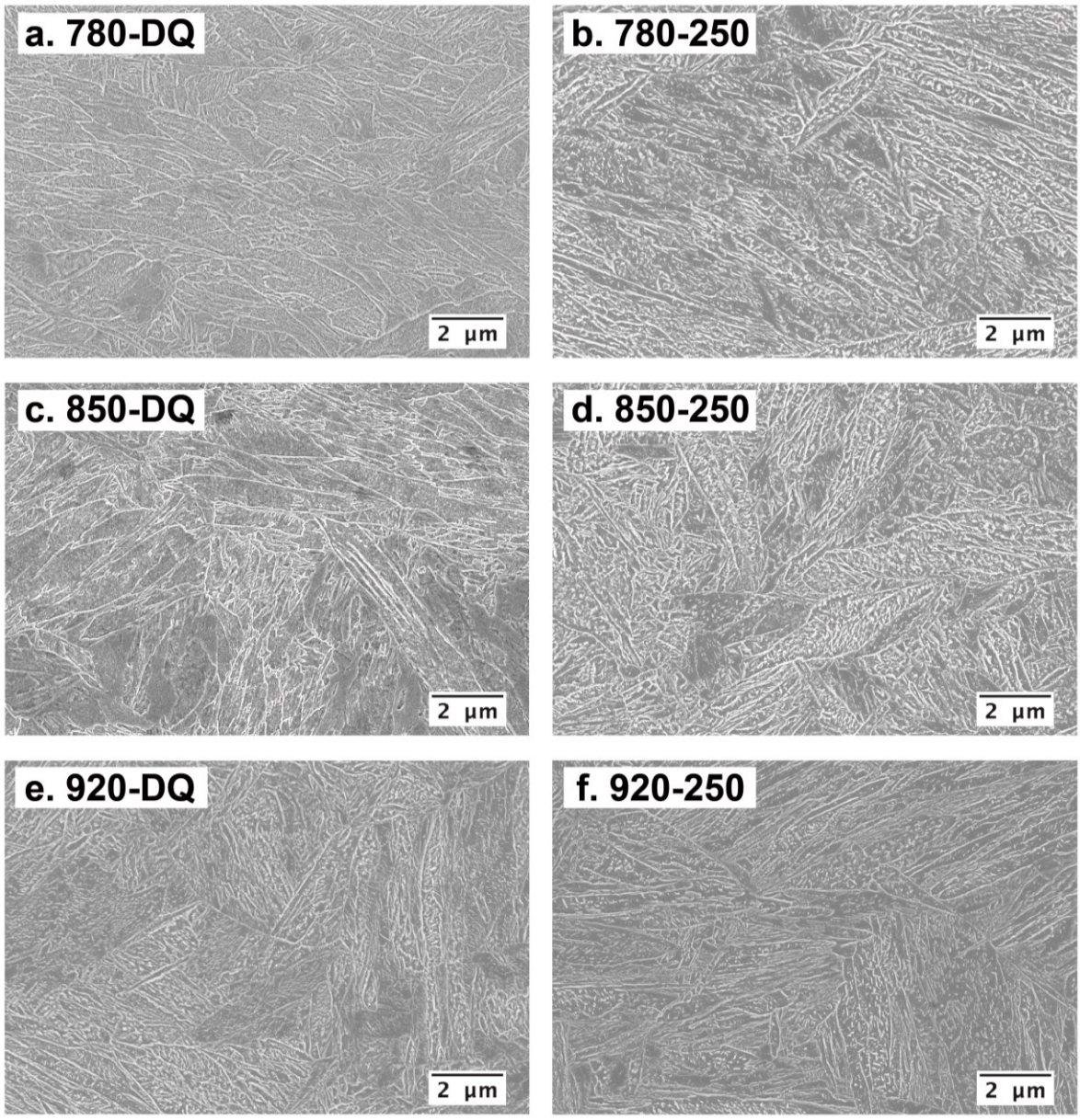

Figure 3. FESEM images of the tested steels.

FESEM images of the microstructures of the tested specimens are given in Figure 3. Lath martensitic structure containing packets and blocks can be distinguished. The figure clearly shows that the variants with a high QFT contain a higher density of carbides, which is to be expected due to the increased autotempering that can occur during the slow cooling from 250 °C. No large islands of retained austenite can be observed in the FESEM images.

Mechanical properties

Surface hardness, material bulk hardness and impact toughness properties for the tested steels are presented in Table 3. Realized finish rolling and quenching finish temperatures are also shown. Average deviation for the surface hardness results was 3.82 %. The highest surface hardness was measured for the direct quenched samples, nearly 700 HV. There were no great differences in the surface hardness values of

Table 3. Realized rolling parameters, average surface hardness values, average material bulk hardness, estimated T28J temperatures, retained austenite content (RA) and average total mass loss during wear testing. Hardness values are given with standard deviation.

Material	FRT (°C)	QFT (°C)	Surface (HV10)	Bulk (HV10)	T28J (°C)	RA (%)
780-DQ	750	20	695±18.4	653±5.7	80	1.9
850-DQ	850	20	680±24.2	637±9.5	100	1.2
920-DQ	890	20	687±17.5	625±11.2	100	1.4
780-250	775	235	648±11.3	617±6.1	-60	3.1
850-250	840	235	611±23.3	598±6.4	-60	3.2
920-250	900	260	505±43.5	580±11.3	-70	2.5

the DQ samples, while bulk average hardness was increased with lower FRT. The interrupted quenching clearly decreased the surface hardness. Almost 200 HV decrease in surface hardness was measured between the 920 DQ and QFT variants. Generally, the surface hardness was greater than the bulk hardness. However, the 920-250 samples showed the opposite trend. This material also showed the largest deviation of individual surface hardness values and wear test mass loss. A possible reason for these material inhomogenities could be the water quenching process: the cooling rate might have been different in some parts of the plate involving temperature gradients.

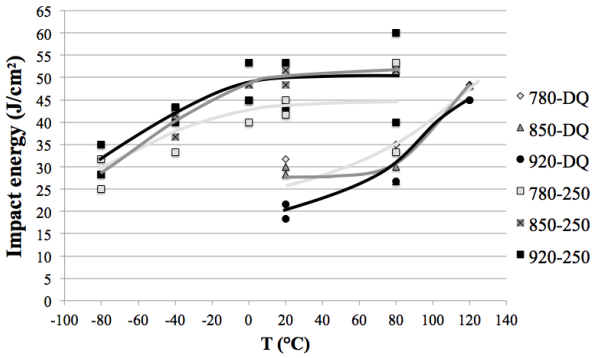

Figure 4. Charpy-V impact test results with transition curves.

Since the Charpy specimens were only ¾ of full width, the results are presented with joules per square centimetre in Figure 4. The impact energy of 35 J/cm^2 corresponds 28 joules with a standard size specimen. Therefore, the T28J temperature was estimated from the plotted curves, but it should be noted that no correlation equations were used for the transition temperature estimation. As only two specimens were tested at each temperature, the estimated transition temperatures are uncertain and transition curves do not represent complete curves due to lack of test points. Nevertheless, comparing the transition temperatures for the DQ and high QFT specimens shows the very strong effect of hardness, i.e. flow stress, on the transition temperature: the bulk hardness difference of 40 HV results in a difference of 160 °C in the transition temperature T28J. Compared to this the effect of FRT is small: a 20 °C improvement in transition temperature for the DQ variants is visible for the lowest FRT, but for the high QFT specimens no clear improvement can be detected.

Impeller-tumbler wear tests

The impeller-tumbler wear test results are given in Table 4. The highest mass loss (0.197 g) was measured for the test variant 920-250 which exhibited the lowest surface hardness (505 HV). The other two QFT variants had quite interestingly nearly the same mass loss despite a 40 HV surface hardness difference. In contrast, all the DQ variants showed very similar hardness values compared to each other, almost attaining the aimed level of 700 HV.

Table 4. Surface hardness and mass loss of the samples with standard deviation.

Material	Surface (HV10)	Mass loss (g)
780-DQ	695±18.4	0.143±0.002
850-DQ	680±24.2	0.148±0.005
920-DQ	687±17.5	0.143±0.004
780-250	648±11.3	0.163±0.004
850-250	611±23.3	0.168±0.001
920-250	505±43.5	0.197±0.008

The wear test results are also in line, and there are no differences regarding mass loss with DQ samples. Figure 5 shows that there is a linear relationship between surface hardness and mass loss (ML). The relationship is as follows:

$$ML = 0.34178 - 0.00028 \times HV10(surface) \quad (1)$$

For this regression equation $R^2 = 0.979$ with a standard error of 0.00336.

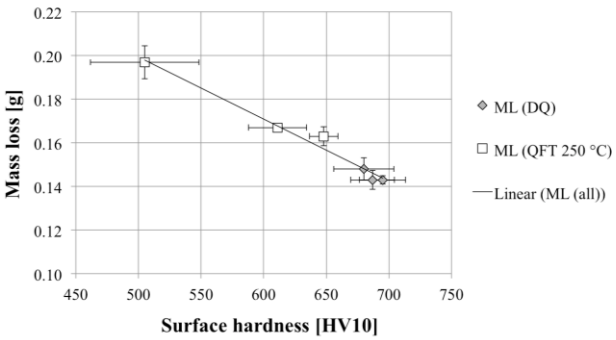

Figure 5. Total mass loss (ML) in the impeller-tumbler wear test as a function of surface hardness with standard deviation for mass loss and surface hardness.

The wear surfaces were examined with both optical and scanning electron microscopes. The impeller-tumbler wear testing device causes heavy wear concentrated on the specimen edges as the samples are rotating inside the tumbler. The worn samples were cut for cross-sectional wear surface inspection, see Figure 6. The direct quenched variants are on the left and the interrupted quenching variants on the right.

Comparing the least (a) and the most (f) worn samples does not clearly reveal any substantial differences. However, a closer examination shows that sample 920-250 (f) has slightly more dented, i.e. rougher edge. It should be noted that the mass loss during the test period is less than 200 milligrams. Surface profile measurements were also done for the worn samples and the results are presented in Table 5. For each material one of the two samples was selected for the surface roughness measurements with the laser scanning confocal microscope. The surface roughness was measured on the flat 12 mm × 9 mm area at 6 mm distance from the tip of the sample and away from the rounded corners. Five measurements were done. The standard for the roughness calculation method was ISO 4287–1997. The surface roughness values are fairly consistent with the measured mass losses showing that roughness increases with increasing mass loss.

Table 5. Measured average surface roughness values for worn samples with standard deviation.

Material	Mass loss (g)	Ra (µm)	Rq (µm)	Rz (µm)
780-DQ	0.143±0.002	6.36±0.04	8.53±0.06	138.5±2.0
850-DQ	0.148±0.005	7.17±0.16	9.63±0.25	143.5±7.2
920-DQ	0.143±0.004	6.50±0.20	8.74±0.31	136.0±3.9
780-250	0.163±0.004	8.07±0.05	10.64±0.07	151.1±6.8
850-250	0.168±0.001	7.60±0.17	10.00±0.25	153.4±5.1
920-250	0.197±0.008	8.45±0.07	11.05±0.11	166.3±9.3

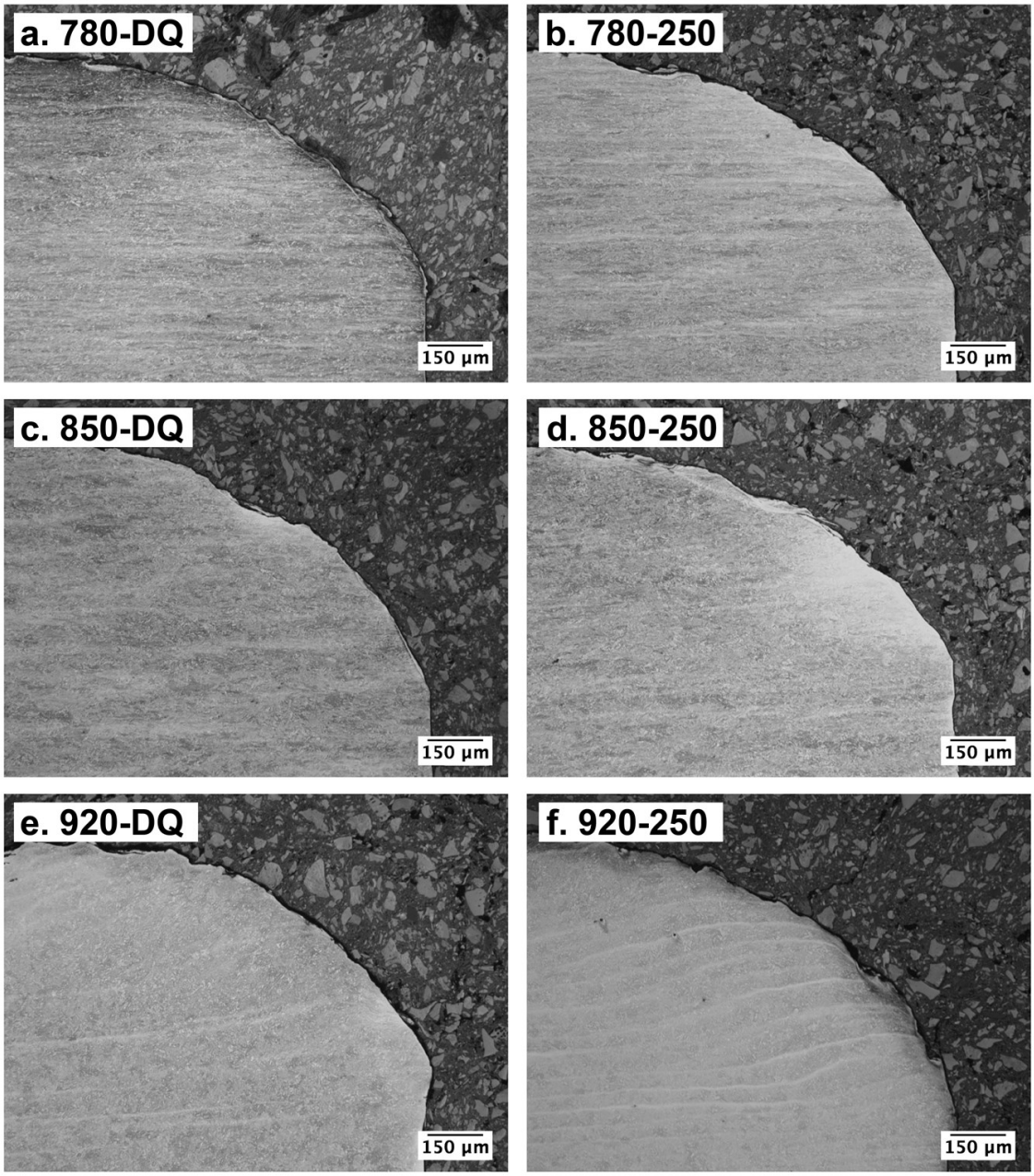

Figure 6. Rounded tips of the impeller-tumbler test specimen.

FESEM images of the worn surfaces and cross-sections of the impeller-tumbler, Figure 7, reveals embedded granite and signs of heavy deformation near the surface. The depth of the affected layer is generally less than 40 µm. Most areas only show a few microns of deformed structure. The high hardness of the steels has clearly prevented greater penetration of the granite. Scratch marks are visible and the wear mode appears to have been mostly abrasive. Cross-sectional images show some larger craters and also some small areas that appear to have been peeled or fractured off the surface.

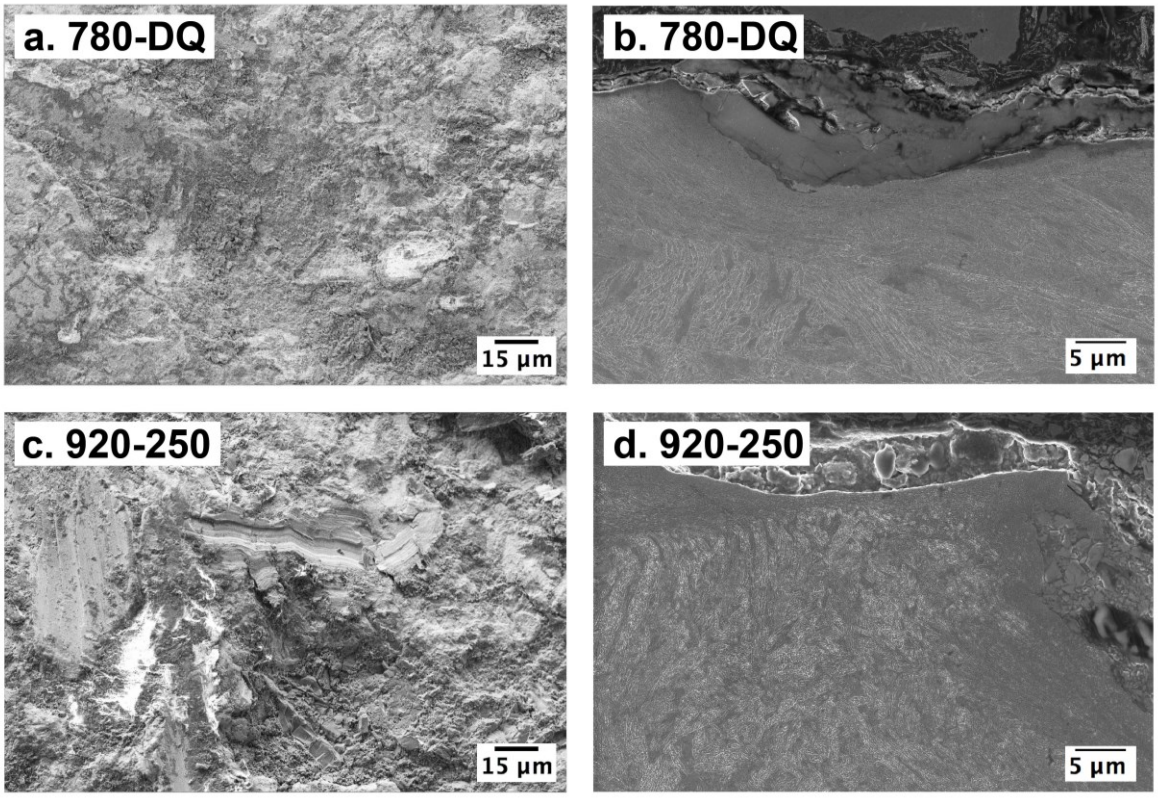

Figure 7. FESEM images of worn surfaces and cross-section of the same specimens: (a) 780-DQ surface, (b) 780-DQ cross-section, (c) 920-250 surface and (d) 920-250 cross-section. (780-DQ is the least worn and 920-250 the most worn of the studied materials).

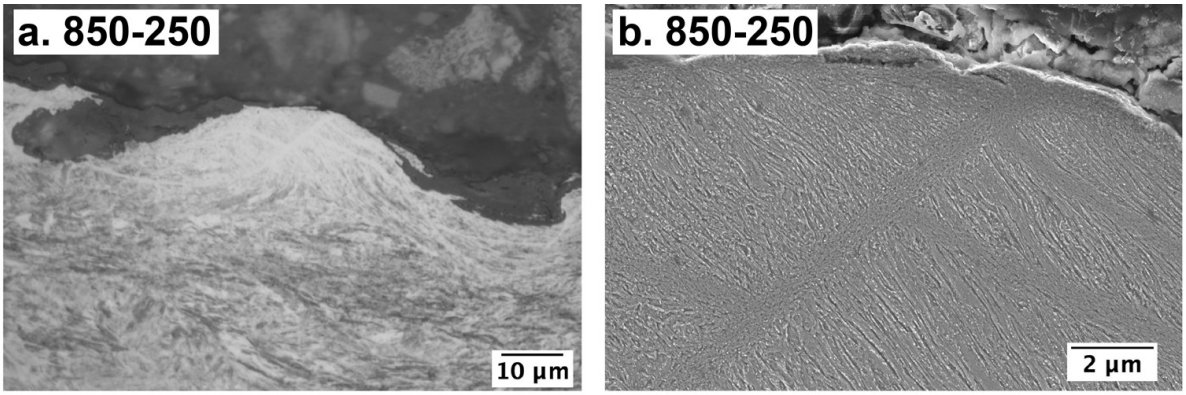

Figure 8. Optical (a) and FESEM (b) image of shear bands (sample 850-250).

Shear bands were discovered in all tested samples. The bands appear white in optical microscope images and darker in FESEM images (Figure 8). Higher magnification examination of the shear bands shows that they contain very fine, nearly nano-sized structure. Another interesting feature is the orientation and fibering phenomenon of the martensite laths in the deformed layer near the surface. The laths have clearly bent and orientated, and they also appear elongated compared to the undeformed laths. The impact energy has been great enough to cause plastic flow in all samples.

DISCUSSION

The rolling schedule was varied to alter the prior austenite grain structure. The aim was to produce more distorted, pancaked grains by rolling in the non-recrystallization regime. The finishing passes at 850 and 780 °C produced elongated grains with higher aspect ratio compared to 920 °C FRT. Calculated T_{nr} was 951 °C. The micrographs of the grain structure support this, as rolling near 900 °C already shows slightly deformed austenite grains. The total reduction (R_{tot}) in the NRX regime and subsequent flat, pancaked grain structure has been attributed to improved impact toughness and strength properties [2–3]. This is derived from the increased total surface area per unit volume ($S_{v(tot)}$) by the amount of austenite grain boundaries and deformation bands of austenite [12]. Work by Kaijalainen et al. [2–3; 12] showed that increased strength, impact toughness and fracture properties for low-carbon direct quenched steels could be achieved by increasing reduction in the NRX regime. Decreasing the FRT from 920 to 860 °C improved the impact energy at -40 °C for medium-carbon abrasion resistant martensitic steel in the work of Deng et al. [13]. Ouchi [1] also notes that increased cumulative rolling below temperature range of austenite recrystallization is utilized to achieve superior low temperature impact toughness with line pipe steels. Thermo-mechanical processing has been already discussed in the 1970's as a novel method for improving impact toughness without loss of strength [14].

Conversely, Bracke et al. [15] reported increased strength and decreased impact toughness for rolling in the non-recrystallization regime. Prior austenite grain aspect ratio between 2 and 4 resulted in deteriorated impact toughness at -20 and -40 °C. However, aspect ratio greater than 4 increased the impact toughness to the same level with the equiaxed grain structure. In this work, the estimated T28J value did show some improvement with decreasing FRT. Though, the amount of impact tests was fairly low and complete transition curves were not plotted. The absolute average values at 20 °C for DQ samples were 20 J/cm^2 for 920-DQ, 29 J/cm^2 for 850-DQ and 25 J/cm^2 for 780-DQ indicating very low toughness in lower temperatures. It is evident in this work that the impact toughness is not drastically changed with the distorted grain structure. This applies to both DQ and QFT samples.

The major improvement with impact toughness was achieved with the interrupted quenching. Stopping the water quenching at 250 °C and subsequent air cooling resulted in lower transition temperatures. All the QFT variants had impact toughness of 20 joules below -40 °C, as none of the DQ samples reached 20 joules below 50 °C. The use of quench finish temperatures above room temperature derived from the novel direct quenching and partitioning process (DQ&P). Q&P processing involves quenching to below M_s temperature to initiate the martensite transformation and then isothermal hold is applied to stabilize the retained austenite [16–17]. In the case of DQ&P, direct quenching to a temperature between M_s and M_f is applied directly after thermomechanical rolling [18], which is what was done in this work. Here, isothermal holding was not applied and the plates were cooled in air after interrupted quenching. This was done in order to simulate industrial processing when isothermal holding is not easily applied. Thomas et al. [5] also discuss non-isothermal partitioning with large coil products. Tan et al. [6] refer to dynamical partitioning when quenching is stopped between M_s and M_f temperatures. The aim in both Q&P and dynamical partitioning is to produce room temperature stable austenite by the partitioning process. This occurs by the diffusion of carbon from martensite to austenite. In dynamical partitioning, the carbon content of the retained austenite is

lower since there is less time for diffusion. However, the lower carbon content of the retained austenite might induce easier transformation to martensite [6]. Thus, the more responsive transformation induced plasticity (TRIP) effects could provide an interesting feature in the dynamically partitioned steels.

The stability and morphology of the retained austenite affect the impact toughness properties. The film-like austenite between laths improves the impact toughness, but granular islands might deteriorate the properties. The effect is related to the finer effective grain size. The film-like austenite will transform under load to martensite with orientation very different from that of the surrounding packet and it does not share the {100} cleavage planes with it [19]. This effect lowers the ductile-to-brittle transformation temperature (DBTT), but does not improve upper shelf impact toughness, i.e. where fracture occurs in a ductile mode. There have also been suggestions that there is an optimum fraction of retained austenite for improved impact toughness. Thus, the best balance between strength, ductility and toughness should be achieved with fine, film-like austenite between the martensite laths with 7–15 % content of retained austenite [20]. In this work no granular islands of retained austenite were observed in the FESEM images. Transmission electron microscope (TEM) would be required to observe the martensite laths with higher resolution.

The QFT samples in this work contained 1.2–3.2 % retained austenite, but impact toughness was improved drastically. The main reason for the improved impact toughness is the lower yield strength, which arises from the combination of the increased austenite content and the autotempering of martensite that accompanies the higher QFT. Brittle fracture in ferritic (including martensitic) steels occurs when the temperature falls to that value where the stress required for plastic flow starts to rise above that required for cleavage [21]. This means that the ductile-to-brittle transformation temperature depends on both yield strength and the stress needed to generate and propagate a cleavage crack through the microstructure. The fracture mode was fully brittle at 20 °C for the tested DQ variants. The QFT variants had mixed ductile-to-brittle fracture at that temperature.

The FESEM images showed that stronger tempering effects have taken place in the QFT samples, but the relatively low quenching finish temperature would suggest the tempering range to be around 200 °C. This would be considered low-temperature tempering and stage I tempering effects occurring. On the microstructural level, this includes the formation of transition carbides and possibly the decomposition of retained austenite. The latter is unlikely to occur in this case due to the carbide formation and due to the constantly decreasing temperature, which leaves little time for the decomposition of austenite. Therefore, the small amount of retained austenite can be considered stable below the quenching finish temperature. As for the changes in the mechanical properties of tempered steels, often low-temperature tempering improves impact toughness with only a small decrease of hardness, which was also observed in the QFT steels. Hence it is difficult to evaluate whether the increased amount of retained austenite or autotempering had greater effect on the yield strength, and also on the impact toughness.

Decreasing the finish rolling temperature seems to affect the surface hardness loss caused by the interrupted quenching. Surface hardness did not decrease as much with the lower finish rolling temperature for the QFT samples. While the impact toughness is almost the same for all QFT samples, there

was a significant drop of hardness with increasing FRT. Thus, the 780-250 variant shows very promising balance of hardness and toughness. The material reached higher than 600 HB surface hardness with impact toughness of around 38 J/cm^2 at -40 °C. However, the realised quenching finish temperature for 920-250 was slightly higher compared to 780-250 and 850-250, which might explain the loss of hardness. Nevertheless, it seems that here the lowest FRT steel preserved the hardness better than the other QFT variants.

The wear performance increases with increasing surface hardness despite drastically deteriorated impact toughness. Figure 5 shows the correlation between hardness and mass loss for the tested impeller-tumbler samples. It is well known that the abrasive wear resistance of steels increases with increasing surface hardness, although the wear performance varies between different microstructures for a given hardness [22–24]. The studied steels all exhibited a martensitic microstructure with slight variations in the small amount of retained austenite. The correlation of mass loss with hardness agrees with other observations in the literature. The major differences in T28J temperature did not affect the wear performance. The toughness at room temperature for all the steels was sufficient to withstand the impact wear caused by the impeller-tumbler. Of course, there is no reason why the notched Charpy-V impact toughness test should be relevant for abrasive wear resistance. Toughness in an abrasive wear sense means tendency to prevent crack propagation, fracture and material detachment [22].

The inspection of the worn surfaces showed that microploughing, microcutting and some microcracking occurred. Abrasive wear had caused distinct marks on the samples and some granite had been embedded to the surfaces. The energy of the impacting particles has been great enough to cause a severely deformed microstructure, although the penetration depth was quite low. Also, shear bands were found in both DQ and QFT samples. The white bands consist of very fine martensite, and are referred to as transformed bands in steels. The adiabatic shear bands have been associated with brittle fracture [27].

Many of the tested steels showed sub-surface shear bands. The directions of the bands vary as some bands were parallel to the elongated grains, but some were perpendicular. Abrasives impact the surface from multiple directions and hence the shear bands may also form in different directions. The surface roughness measurements also prove that the samples with greater mass loss have a rougher surface. The greatest difference was measured for the R_z values (the absolute vertical distance between the highest peak and the deepest valley) that were significantly higher for the most worn samples. The high R_z values indicate that there are deeper scratches or valleys on the sample surface. Also, both R_a and R_q were higher for the more worn samples.

Strong fibering of martensite laths was observed near the surface (Figure 9). This has been observed earlier in the impeller-tumbler tests with 400–650 HB hardness grade steels [28], but also in crushing pin-on-disk tests with 400 HB wear-resistant steels [29]. Very fine microstructure could be seen near the surface, similar to the shear band structure, often referred as a white layer. This indicates that brittle fracture has happened and some parts of the surface layer might have fractured and peeled off. Comparison between the most worn (920-250) and the best performing sample (780-DQ) shows that there is more coverage by white layer on the surface of the 920-250 and the layer is also thicker. In contrast, the 780-DQ has much smoother surface with less white deformed sections. Sample 920-250 seems to have work

hardened more, but this has not prevented the cracking of the surface.

It has been suggested that some softer steels show better wear performance due to good work hardening capability, but the transition from hard tribolayer to bulk should be smooth [29]. Now the hard layer can be cracked by the repeated impacts. Figure 10 shows an embedded granite particle and cracked white layer in sample 920-250. Softer multi-phase microstructures have proven to be better against two-body abrasive wear when compared to same hardness level single-phase martensitic steels [24]. However, here it seems that softer martensitic structure forms thicker white tribolayer than the harder martensite. The white layer then cracks and peels off due to impact wear. Significantly harder samples prevented the formation of the brittle surface layer and withstood more impacts and grooving.

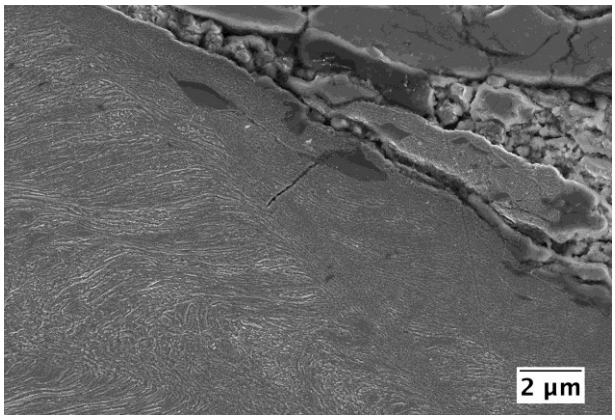

Figure 9. FESEM image of martensite laths bending and fibering (sample 850-250).

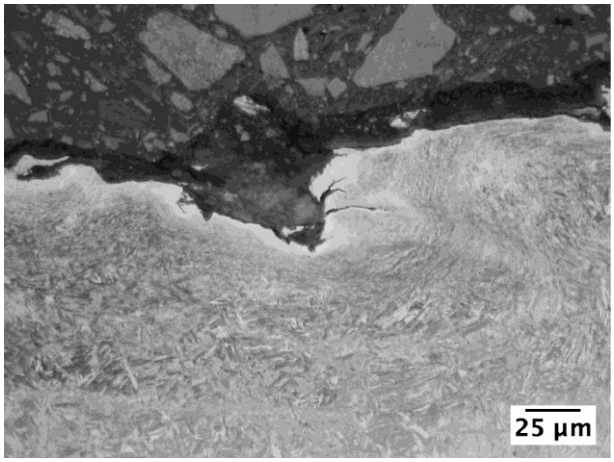

Figure 10. Optical microscope image of sample 920-250 with embedded granite particle.

The current tests showed that the highest initial surface hardness provided the best wear performance in laboratory scale impact-abrasion tests. Direct quenching produced high hardness values while interrupted quenching resulted in lower hardness, but better impact toughness. The composition was the same for all tested steel variants, and all variants had martensitic microstructure. The outcome of the current paper is that the wear rate is lowest for the hardest martensitic steels, but it was shown that an ultra-high strength steel with well-balanced impact toughness and hardness properties can be produced by novel interrupted quenching method combined with thermomechanically controlled processing.

CONCLUSIONS

The present work has shown that hardness is the main factor controlling the abrasive wear of medium carbon martensitic steels in the impeller-tumbler test. Processing method was thermomechanically controlled processing (TMCP) with different finish rolling temperatures (FRT). Direct quenching (DQ) and interrupted quenching with quenching finish temperature (QFT) of 250 °C were applied. Nearly 700 HV surface hardness was

achieved with the direct quenched samples. All tested steel variants had a martensitic microstructure.

Varying the finish rolling temperature (920, 850 and 780 °C) resulted in different prior austenite grain size and shape. Decreasing the FRT produced elongated and more pancaked grain structure. However, the impact toughness was not significantly improved by rolling in the non-recrystallization (NRX) regime.

The interrupted quenching provided greater impact toughness values which is attributed to the autotempering effects and increased amount of retained austenite. The direct quenched variants showed low toughness even at room temperature. In contrast, the surface hardness was lower for the QFT variants. The best balance of impact toughness and hardness was achieved with 780 °C FRT combined with 250 °C QFT.

The high hardness prevented the penetration of abrasives into the surface. Brittle tribolayer was formed on the surface of the samples with lower hardness, which seemed to fracture under impact wear. Adiabatic shear bands were discovered on all samples.

ACKNOWLEDGEMENTS

The research described has been done within *Breakthrough Steels and Applications* (*BSA*) program of DIMECC Ltd. We gratefully acknowledge financial support from the Finnish Funding Agency for Technology and Innovation (Tekes) and the companies participating in the above programs. The corresponding author would also like to express his gratitude for the support provided by the University of Oulu Graduate School through the Advanced Materials Doctoral Program (ADMA-DP).

REFERENCES

1. C. Ouchi. Development of Steel Plates by Intesive Use of TMCP and Direct Quenching Processes. ISIJ International 41(6) (2001), pp. 542–553.
2. A.J. Kaijalainen, P.P. Suikkanen, T.J. Limnell, L.P. Karjalainen, J.I. Kömi, D.A. Porter. Effect of austenite grain structure on the strength and toughness of direct-quenched martensite. Journal of Alloys and Compounds 577S (2013), pp. 642–648.
3. A.J. Kaijalainen, P.P. Suikkanen, L.P. Karjalainen, J.J. Jonas. Effect of Austenite Pancaking on the Microstructure, Texture and Bendability of an Ultrahigh-Strength Strip Steel. Metallurgical and Materials Transactions A 45A (2014), pp. 1273–1283.
4. E. Kinnunen, I. Miettunen, M.C. Somani, D.A. Porter, L.P. Karjalainen, I. Alamattila, A. Kemppainen, T. Liimatainen, V. Ratia. Development of a New Direct Quenched Abrasion Resistant Steel. International Journal of Metallurgical Engineering 2(1) (2013), pp. 27–34.
5. G.A. Thomas, J.G. Speer, D.K. Matlock. Quenched and Partitioned Microstructures Produced *via* Gleeble Simulations of Hot-Strip Mill Cooling Practices. Metallurgical and Materials Transactions A 42A (2011), pp. 3652–3659.
6. X. Tan, Y. Xu, X. Yang, Z. Liu, D. Wu. Effect of partitioning procedure on microstructure and mechanical properties of a hot-rolled directly quenched and partitioned steel. Materials Science & Engineering A 594 (2014), pp. 149–160.
7. F. Tariq, A. Baloch. One-Step Quenching and Partitioning Heat Treatment of Medium Carbon Low Alloy Steel. Journal of Materials Engineering and

Performance 23(5) (2014), pp. 1726–1739.

8. V. Ratia, K. Valtonen, A. Kemppainen, V-T. Kuokkala. High-Stress Abrasion and Impact-Abrasion Testing of Wear Resistant Steels. Tribology Online 8(2) (2013), pp. 152–161.
9. G. Krauss. Steels: Processing, Structure, and Performance. ASM International, 2005. 613 p.
10. R. Barbosa, F. Boratto, S. Yue, J.J. Jonas. The influence of chemical composition on the recrystallization behaviour of microalloyed steels, in: THERMEC '88. Proceedings. Iron and Steel Institute of Japan, Tokyo, 1988, p. 383–390.
11. R.L. Higginson, C.M. Sellars. Worked examples in quantitative metallography. Maney Publishing, 2003. 128 p.
12. A.J. Kaijalainen, P.P. Suikkanen, L.P. Karjalainen, J.I. Kömi, A.J. DeArdo. Effect of austenite conditioning in the non-recrystallization regime on the microstructures and properties of ultra-high strength bainitic/martensitic strip steel, in: 2nd International Conference on Super-high Strength Steels, Verona, 2010. 19 p.
13. X. Deng, Z. Wang, Y. Han, H. Zhao, G. Wang. Microstructure and Abrasive Wear Behavior of Medium Carbon Low Alloy Martensitic Abrasion Resistant Steel. Journal of Iron and Steel Research International 21 (1) (2014), pp. 98–103.
14. I. Kosazu, C. Ouchi, T. Sampei, T. Okita. Hot Rolling as a High-Temperature Thermo-Mechanical Process. In: Proc. Int. Symp. Microalloying '75, Union Carbide Corporation, New York, USA 1975, pp. 100–114.
15. L. Bracke, W. Xu, T. Waterschoot. Effect of finish rolling temperature on direct quenched low alloy martensite properties. Materials Today: Proceedings 2s (2015), pp. S659–S662.
16. J. Speer, D.K. Matlock, B.C. De Cooman, J.G. Schroth. Carbon partitioning into austenite after martensite transformation. Acta Materialia 51 (2003), pp. 2611–2622.
17. D.V. Edmonds, K. He, F.C. Rizzo, B.C. De Cooman, D.K. Matlock, J.G. Speer. Quenching and partitioning martensite – A novel steel heat treatment. Materials Science and Engineering: A 438–440 (2006), pp. 25–34.
18. M.C. Somani, D.A. Porter, L.P. Karjalainen, P.P. Suikkanen, R.D.K. Misra. Process design for tough ductile martensitic steels through direct quenching and partitioning. Materials Today: Proceedings 2S (2015), pp. S631–S634.
19. J.I. Kim, C.K. Syn, J.W. Morris. Microstructural sources of toughness in QLT-Treated 5.5Ni cryogenic steel. Metallurgical Transactions A 14(1) (1983), pp. 93–103.
20. P.P. Suikkanen, A-J. Ristola, A.M. Hirvi, P. Sahu, M.C. Somani, D.A. Porter, L.P. Karjalainen. Effects of Carbon Content and Cooling Path on the Microstructure and Properties of TRIP-aided Ultra-High Strength Steels. ISIJ International 53(2) (2013), pp. 337–346.
21. J.W. Morris. Metallurgical control of the ductile-brittle transition in high-strength structural steels, in: Proceedings of the 1998 MRS Fall Meeting - The Symposium Advanced Catalytic Materials, Boston, MA, USA, 1998. Materials Research Society Symposium, Proceedings, 539 (1999), pp. 23–27.
22. A. Sundström, J. Rendon, M. Olsson. Wear behaviour of some low alloyed steels under combined impact/abrasion

contact conditions. Wear 250 (2001), pp. 744–754.

23. J. Rendon, M. Olsson. Abrasive wear resistance of some commercial abrasion resistant steels evaluated by laboratory test methods. Wear 367 (2009), pp. 2055–2061.
24. B. Narayanaswamy, P. Hodgson, H. Beladi. Comparisons of the two-body abrasive wear behaviour of four different ferrous microstructures with similar hardness levels. Wear 350–351 (2016), pp. 155–165.
25. P.I. Patil, R.G. Tated. Comparison of Effects of Cryogenic Treatment on Different Types of Steels: A Review. In: Proceedings on International Conference in Computational Intelligence (ICCIA March 2012). ICCIA (9), pp. 10–29.
26. E. Vuorinen, N. Ojala, V. Heino, C. Rau, C. Gahm. Erosive and abrasive wear performance of carbide free bainitic steels – comparison of field and laboratory experiments. Tribology International 98 (2016), pp. 108–115.
27. B. Dodd, Y. Bai. Adiabatic Shear Localization. Elsevier, 2012. 468 p.
28. V. Ratia, I. Miettunen, V-T. Kuokkala. Surface deformation of steels in impact-abrasion: The effect of sample angle and test duration. Wear 301 (2013), pp. 94–101.
29. N. Ojala, K. Valtonen, V. Heino, M. Kallio, J. Aaltonen, P. Siitonen, V-T. Kuokkala. Effects of composition and microstructure on the abrasive wear performance of quenched wear resistant steels. Wear 317 (2014), pp. 225–232.